

A Statistical Framework for Elastic Shape Analysis of Spatio-Temporal Evolutions of Planar Closed Curves

Chafik Samir
LIMOS CNRS UMR 6158
University of Clermont Auvergne
Clermont Ferrand, France
chafik.samir@udamail.fr

Sebastian Kurtek
Department of Statistics
The Ohio State University
Columbus, OH, USA
kurtek.1@stat.osu.edu

Justin Strait
Department of Statistics
The Ohio State University
Columbus, OH, USA
strait.50@osu.edu

Shantanu H. Joshi
Department of Neurology, UCLA Brain Mapping Center
University of California, Los Angeles
Los Angeles, CA, USA
s.joshi@ucla.edu

Abstract

We propose a new statistical framework for spatio-temporal modeling of elastic planar, closed curves. This approach combines two recent frameworks for elastic functional data analysis and elastic shape analysis. The proposed trajectory registration framework enables matching and averaging to quantify spatio-temporal deformations while taking into account their dynamic specificities. A key ingredient of this framework is a tracking method that optimizes the evolution of curves extracted from sequences of consecutive images to estimate the spatio-temporal deformation fields. Automatic estimation of such deformations including spatial changes (strain) and dynamic temporal changes (phase) was tested on simulated examples and real myocardial trajectories. Experimental results show significant improvements in the spatio-temporal structure of trajectory comparisons and averages using the proposed framework.

1. Introduction

Recent advances in imaging technology have led to an increased need for image registration methods which are used in a large number of applications including medical imaging, computer vision, augmented reality, etc. The image registration problem consists of mapping a target image to a reference image under certain transformation constraints. The estimated deformation can be based on intensity (gray-scale level correspondences), geometry (features or landmarks) or both [7]. However, most of these meth-

ods are applied in a cross-sectional manner, i.e., they ignore any temporal structure contained in data sequences and deal only with the static spatial information. The development of techniques for spatio-temporal tracking and deformation will enable one to capture both the local shape and temporal variabilities under a unified framework [3]. Such spatio-temporal registration methods incorporate the construction of a statistical model in order to account for the cross-sectional geometric variability of object shapes and the additional functional dynamics. In the case of medical imaging, such models can assist physicians in the interpretation of image sequences. For example, they can be used to guide disease characterization via image sequence classification and unsupervised segmentation [2]. As an ultimate goal, one can perform statistical comparisons between individuals and groups to help produce efficient clinical tools.

In order to build a statistical model from image sequences describing both the shape and dynamics of an object, the following issues must be addressed: (i) Spatial registration (**local shape differences**): How to capture the spatial variability for observations at a specific instance in time? (ii) Temporal registration (**temporal shape differences**): How to capture the dynamics during a sequence of shape evolution?, and (iii) Inter-subject variability: fixing the observation period, how to build a reference model for comparison? and finally how to capture differences in shape trajectories caused by deformation during that period? In this spirit, we present a new trajectory-based registration/statistical modeling approach that can automatically register curve sequences observed during a common time period to study their developmental and spatio-temporal

variability. Our method is applicable to modeling soft tissue motion and deformation, and motivated by spatio-temporal mechanical models. Soft tissue was first modeled as a linear model in order to apply continuum mechanical constraints, and then extended to nonlinear material models (viscoelastic or hyperelastic) for more accuracy [1]. Due to low complexity and easy implementation of the linear models, these methods have been widely used in applications, but their performance is very limited [4].

In the last decade, there have been many efforts to accurately model soft tissue motion and deformation in general settings. In soft tissue modeling, several models were proposed including elastic, viscoelastic, and hyperelastic models [12]. Most of the presented solutions are based on general models and were implemented with a wide range of computational methods. Among others, we can cite variational methods and finite-element methods, spatio-temporal B-splines, and deformable models [13, 2]. Specifically, variational formulations have been mainly used to regularize ill-conditioned problems in several applications including medical imaging. In this study, we propose to model the soft tissue motion as trajectories on an elastic shape space in order to capture main disease characteristics: trajectory dynamics and spatial strain. Hence, both spatial and temporal registration is considered in our analysis. Recent methods that have considered statistical analysis of shape trajectories, and accounted for their spatio-temporal variability, include [10] and [11]. Both of these methods focused on applications to activity recognition and applied to single shapes at each time along the trajectory. In this paper, we are motivated by the problem of analyzing myocardial trajectories, which contain endo- (inside) and epi- (outside) cardiac boundaries, thus resulting in temporal evolutions of two shapes.

This paper is organized as follows. Section 2 describes the preliminaries needed for statistical analysis of spatio-temporal trajectories. Section 3 presents the proposed framework. Section 4 gives results on simulated and real data followed by a short summary (Section 5).

2. Elastic Statistical Shape Analysis of Curves

In this work, we develop a new framework for statistical shape analysis of temporal evolutions of planar, closed curves. In particular, we address the problem of spatio-temporal registration of such trajectories. We split the spatio-temporal registration problem into two steps: (1) we perform temporal registration of the shape trajectories using a scalar feature invariant to shape preserving transformations, and (2) we perform cross-sectional spatial registration by removing all shape preserving transformations from the representation space. The temporal registration is performed using ideas from elastic functional data analysis [9, 6]. The spatial registration applies elastic shape analysis

of planar, closed curves [8]. We provide short descriptions of these two methods in the following sections, and subsequently present a unified framework for analyzing spatio-temporal myocardial trajectories.

2.1. Elastic Functional Data Analysis

Without loss of generality, let f be a real-valued, absolutely continuous function with the domain $[0, 1]$. Let \mathcal{F} denote the set of all such functions and Γ be the set of orientation-preserving diffeomorphisms of $[0, 1]$. Elements of Γ are used to represent temporal variability of functions. In order to register two given functions f_1 and f_2 , we take an approach based on the square-root slope function (SRSF) representation $q : [0, 1] \rightarrow \mathbb{R}$ defined as $q(t) = \text{sign}(\dot{f}(t))\sqrt{|\dot{f}(t)|}$, where \dot{f} is the derivative of f [9, 6]. If the function f is absolutely continuous, the resulting SRSF is square-integrable. Furthermore, if we temporally warp a function f by $\gamma \in \Gamma$, the SRSF of $f \circ \gamma$ is given by $\tilde{q} = (q, \gamma) = (q \circ \gamma)\sqrt{\dot{\gamma}}$. The main motivation for using the SRSF for temporal registration of functional data is that, under this representation, Γ acts on \mathcal{F} by isometries under the \mathbb{L}^2 metric, i.e., $\|q_1 - q_2\| = \|(q_1, \gamma) - (q_2, \gamma)\|$. This property is necessary to define a proper metric, which can be used as a cost function to temporally register two or multiple functions.

Pairwise alignment of functions can be performed by utilizing equivalence classes of the form: $[q] = \{(q, \gamma) | \gamma \in \Gamma\}$. Under this setup, any two functions within the same temporal warping of each other are considered equivalent (i.e., any two functions in the set $[q]$ differ only in their temporal alignment). The space of all equivalence classes is denoted by $\mathcal{Q} = \{[q]\}$. To temporally register two functions (compare any two equivalence classes), we use the \mathbb{L}^2 metric on the space of SRSFs as follows. For any two functions $f_1, f_2 \in \mathcal{F}$ and their corresponding SRSFs, q_1, q_2 , we define the warping invariant distance between them as $d_{\mathcal{Q}}([q_1], [q_2]) = \inf_{\gamma \in \Gamma} \|q_1 - (q_2 \circ \gamma)\sqrt{\dot{\gamma}}\|$. The minimizer of $d_{\mathcal{Q}}$ is denoted by γ^* and represents the optimal temporal alignment of f_2 to f_1 . This optimization can be solved using a dynamic programming algorithm.

An important goal of the proposed framework is to align multiple functions simultaneously for the purposes of temporal registration of multiple trajectories. This is accomplished using the notion of the Karcher mean. For a sample of functions f_1, f_2, \dots, f_n , let q_1, q_2, \dots, q_n denote their SRSFs. Then, their Karcher mean is defined as $[\bar{q}] = \arg \min_{[q] \in \mathcal{Q}} \sum_{i=1}^n d_{\mathcal{Q}}([q], [q_i])^2$. The Karcher mean is actually an equivalence class of functions, and we choose a representative element of this equivalence class using the orbit centering method (see [9] for details). This procedure results in three items: (1) \bar{q} , the preferred element of the Karcher mean equivalence class, (2) $\{\gamma_i^*\}$, the set of optimal temporal alignment functions, and (3) $\{f_i^* = f_i \circ \gamma_i^*\}$,

the set of temporally aligned functions.

2.2. Elastic Size-and-Shape Analysis of Planar, Closed Curves

The framework of Srivastava et al. [8, 5] provides tools for spatial alignment, comparison and averaging of planar, closed curves. We provide a brief description of the relevant methods, and refer the reader to the original paper for details. Let $\beta : \mathbb{S}^1 \rightarrow \mathbb{R}^2$ denote a planar closed curve. In order to study shapes of closed curves, we impose a condition, which ensures that each β starts and ends at the same point. Its corresponding square-root velocity function (SRVF) representation is defined as $m(s) = \frac{\dot{\beta}(s)}{\sqrt{|\dot{\beta}(s)|}}$, where $\dot{\beta}$ is the derivative of β and $|\cdot|$ is the Euclidean norm. As in the case of functions presented in the previous section, the curve β can be uniquely recovered from its SRVF up to a translation. We are interested in modeling size and shape of myocardial curves, and thus, we seek a representation that is invariant to translation, rotation, and re-parameterization. The SRVF representation is automatically invariant to translation (it only depends on $\dot{\beta}$). The shape space of planar, closed curves is obtained by removing the re-parameterization group denoted by Λ (the set of diffeomorphisms from \mathbb{S}^1 to itself) and rotation group $SO(2)$ using equivalence classes of the form: $[m] = \{O(m \circ \lambda)\sqrt{\lambda} | O \in SO(2), \lambda \in \Lambda\}$. The shape space is then defined as $\mathcal{S} = \{[m]\}$. The motivation for using the SRVF representation for modeling shapes of curves is similar to the function case discussed earlier, i.e., Λ acts on the SRVF space by isometries under the \mathbb{L}^2 metric.

Shape comparisons can be achieved by comparing the corresponding equivalence classes of SRVFs in the following manner. For two curves β_1 and β_2 , represented using their SRVFs m_1 and m_2 , the shape distance between them is given by $d_{\mathcal{S}}([m_1], [m_2]) = \inf_{O \in SO(2), \lambda \in \Lambda} \|m_1 - O(m_2 \circ \lambda)\sqrt{\lambda}\|$, where $\|\cdot\|$ is the \mathbb{L}^2 norm. This shape distance can be used to define a shape average for a collection of curves β_1, \dots, β_n , represented using their SRVFs m_1, \dots, m_n , using the notion of the Karcher mean: $[\bar{m}] = \arg \min_{[m] \in \mathcal{P}} \sum_{i=1}^n d_{\mathcal{S}}([m], [m_i])^2$. Any element of the Karcher mean orbit can be selected to represent its overall shape (see [8] for details).

3. Spatio-temporal Registration, Comparison and Averaging of Trajectories

In this section, we unify the methods presented in Sections 2.1 and 2.2 to define a framework for spatio-temporal modeling of myocardial trajectories. Let η_1 and η_2 represent two temporal trajectories of closed, planar curves. The first trajectory η_1 represents the evolution of the outer boundary of the myocardium (denoted β_O), while the sec-

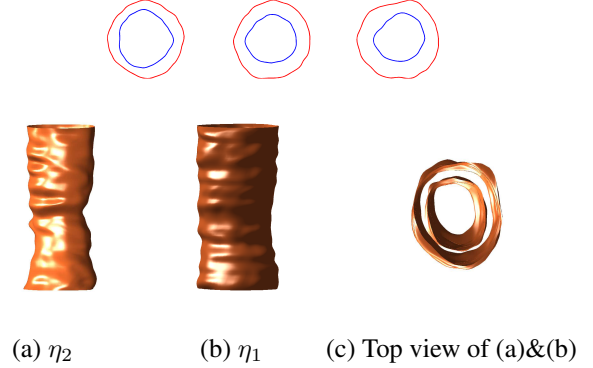


Figure 1. Top: Myocardial wall boundaries extracted from image sequences. (a)&(b) Full inner and outer trajectories (η_2 and η_1), respectively. (c) Top view of the combined trajectory.

ond trajectory η_2 represents the evolution of the inner boundary (denoted β_I) (see Figure 1 for an example). Given two sets of such myocardial trajectories, $\eta^1 = (\eta_1^1, \eta_2^1)$ and $\eta^2 = (\eta_1^2, \eta_2^2)$ coming from two different subjects, the first step in our analysis is to find their optimal temporal alignment. For this purpose, we utilize the temporal function of average areas enclosed by the inner and outer boundaries. Let $A_O(t)$ and $A_I(t)$ denote the areas enclosed by the outer and inner myocardial curves at time t along the trajectory. These two quantities can be easily computed and are invariant to common translation and rotation, and re-parameterization of the myocardial curves. For each η^j , $j = 1, 2$ we form a univariate function $A^j = (A_O^j + A_I^j)/2$ and use the elastic functional data analysis framework described in Section 2.1 to estimate the optimal temporal alignment of the trajectories, denoted by γ^* , based on the average area functions A^1 and A^2 . We then apply γ^* to η^2 resulting in $\eta^{2*}(t) = (\eta_1^2(\gamma^*(t)), \eta_2^2(\gamma^*(t)))$.

Once the two trajectories are temporally aligned, we perform spatial alignment in a cross-sectional manner using the elastic size-and-shape analysis framework presented in Section 2.2. Then, the distance between two temporally aligned myocardial trajectories is given by $d(\eta^1, \eta^{2*}) = \sum_{j=1}^2 \int_0^1 d_{\mathcal{S}}([\eta_j^1(t)], [\eta_j^{2*}(t)]) dt$. We make the following small adjustment at the implementation stage: the optimal rotation and seed placement are found jointly for the inner and outer myocardial boundaries. This enforces consistency between the two boundaries. Optimal re-parameterizations are determined individually.

Averaging can be performed in a similar manner. Given a set of myocardial trajectories η^1, \dots, η^n , we begin by computing the average area functions A^1, \dots, A^n . We then perform multiple function alignment using the Karcher mean resulting in the warping functions $\gamma_1^*, \dots, \gamma_n^*$. These are subsequently applied to the myocardial trajectories resulting in $\eta^{j*}(t) = (\eta_1^j(\gamma_j^*(t)), \eta_2^j(\gamma_j^*(t)))$, $j = 1, \dots, n$. After

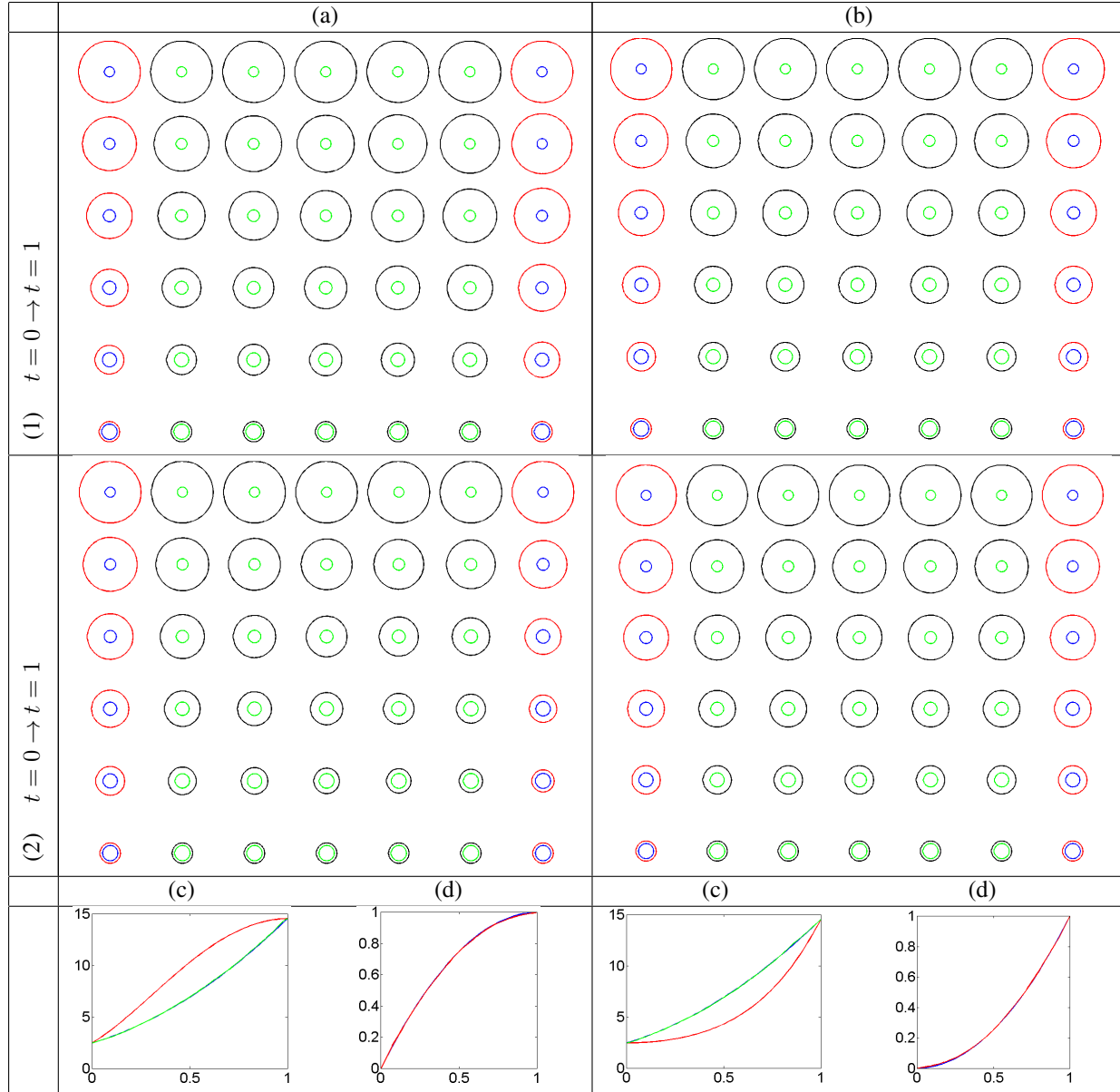


Figure 2. Two comparisons ((1)-(2)) of simulated trajectories with temporal variability only. (a) Linear interpolation before spatio-temporal alignment. (b) Shape geodesic after alignment. In both panels, the red and blue curves denote the two given trajectories while the black and green ones give the interpolations. Each trajectory begins with $t = 0$ at the bottom of the plot and ends with $t = 1$ at the top of the plot with equal time sampling in-between. (c) The average area function for trajectory 1 (blue), trajectory 2 before alignment (red) and after alignment (green). (d) True temporal warping in blue and recovered temporal warping in red. ((1)=left, (2)=right).

temporal registration, we perform cross-sectional averaging of the inner and outer myocardial shapes using the Karcher mean on the shape space \mathcal{S} .

4. Experimental Results

In this section, we present comparison and averaging results on synthetic and real data.

4.1. Simulations

Simulation 1: Temporal Registration. In the first simulation, we study how well we can recover temporal variability between two trajectories. For this purpose, we generate a trajectory where the inside and outside boundaries are concentric circles with varying radii. Then, we simulate two different temporal warpings: $\gamma_1 = t + 0.99t(1 - t)$ and $\gamma_2 = t - 0.99t(1 - t)$. For each test, we apply one of the

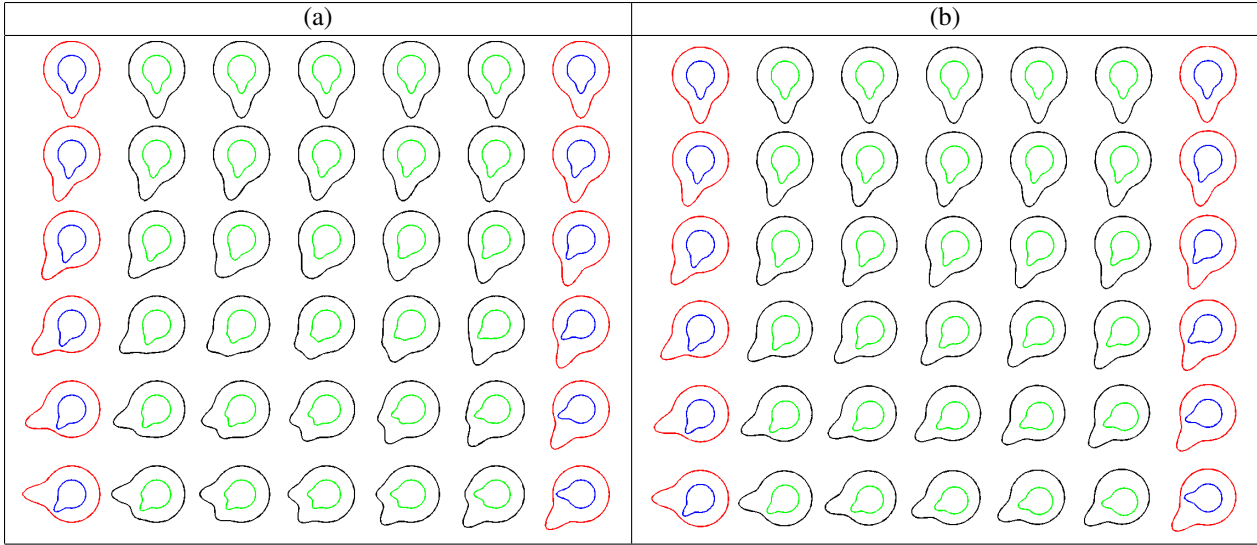


Figure 3. A comparison of two simulated trajectories with spatial variability only. (a) Linear interpolation before spatio-temporal alignment. (b) Shape geodesic after alignment. In both panels, the red and blue curves denote the two given trajectories while the black and green trajectories give the interpolations. Each trajectory begins with $t = 0$ at the bottom of the plot and ends with $t = 1$ at the top of the plot with equal time sampling in-between.

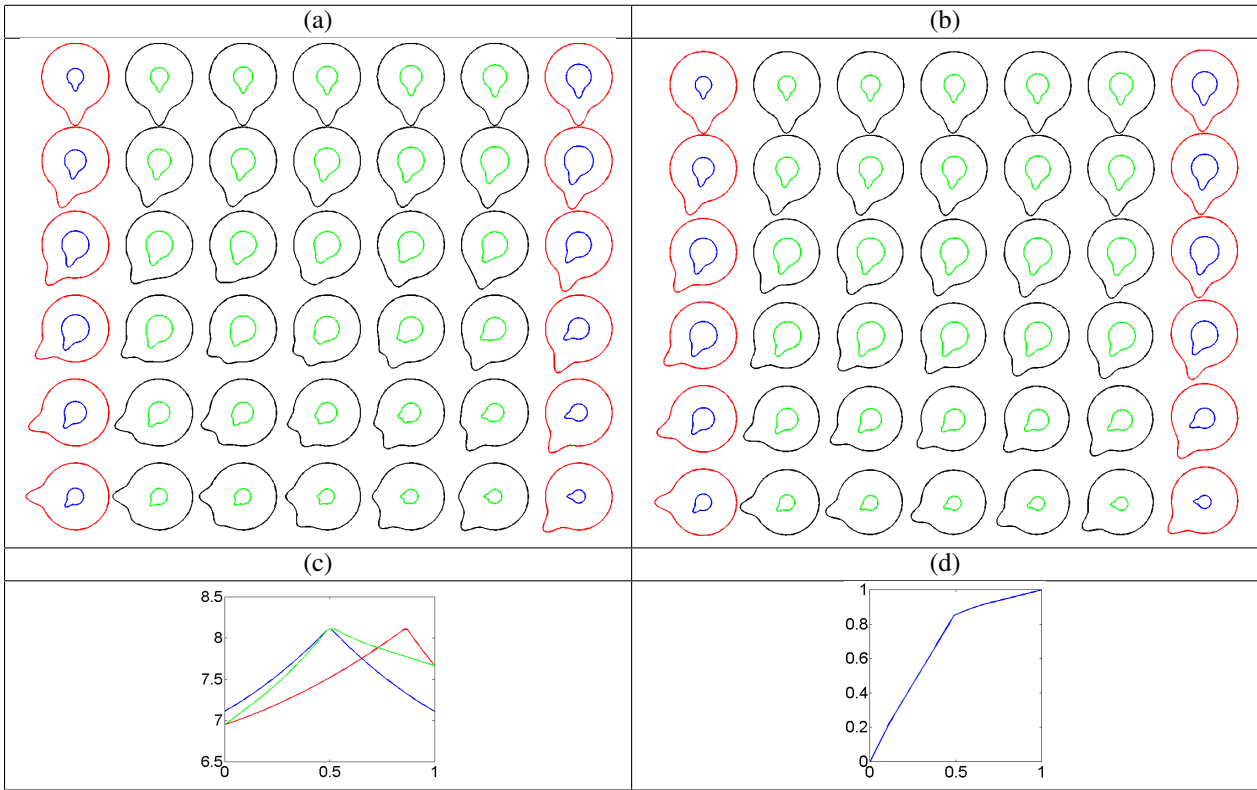


Figure 4. A comparison of two simulated trajectories with spatio-temporal variability. (a) Linear interpolation before spatio-temporal alignment. (b) Shape geodesic after alignment. In both panels, the red and blue curves denote the two given trajectories while the black and green trajectories give the interpolations. Each trajectory begins with $t = 0$ at the bottom of the plot and ends with $t = 1$ at the top of the plot with equal time sampling in-between. (c) The average area function for trajectory 1 (blue), trajectory 2 before alignment (red) and after alignment (green). (d) Temporal warping function.

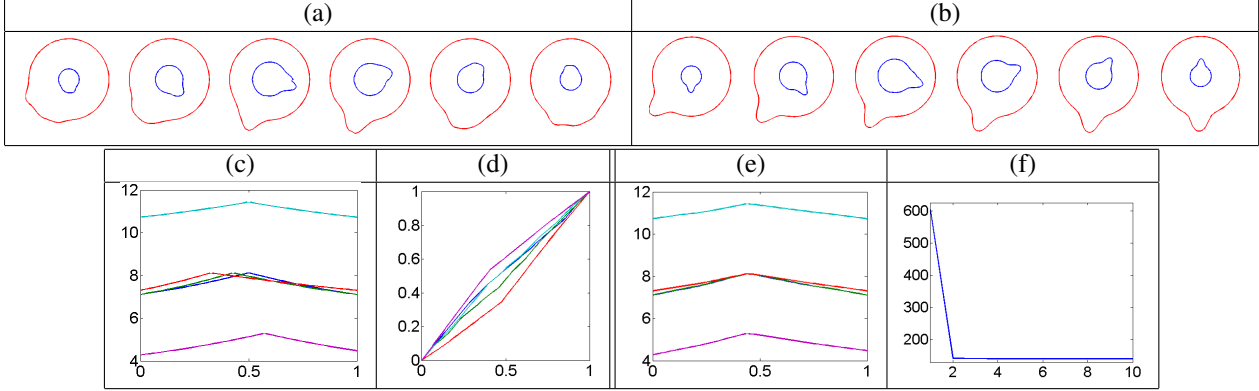


Figure 5. Averaging of trajectories with spatio-temporal variability. (a) Cross-sectional average without spatio-temporal alignment. (b) Average computed using the proposed method. Each trajectory begins with $t = 0$ and ends with $t = 1$ (left to right). (c) Average area functions for the five trajectories prior to temporal alignment. (d) Temporal warping functions. (e) Average area functions after temporal alignment. (f) Evolution of the algorithm energy (average variance).

warpings to the generated trajectory and apply our comparison method. In each case, we expect the distance between the two trajectories to be exactly zero since they are within a temporal warping of each other. The results are presented in Figure 2. The proposed method is very accurate at recovering the true temporal variation, even in the presence of severe warping as in the given examples. In Example (1), the initial distance between the two trajectories is 0.3202, which reduces to 0.0055 once the trajectories are temporally aligned. In Example (2), the initial distance between the two trajectories is 0.3561, which reduces to 0.0058 after alignment. In both cases, the distance decreases by over 98% and is very close to zero, as expected. This is reflected in the interpolation plots in panels (a) and (b). In panel (b), the geodesic interpolations constitute nearly constant paths, which is consistent with the very low distance. Panel (c) displays the average area functions for the two trajectories before and after temporal alignment. The functions are nearly identical once temporal registration is accounted for. Panel (d) confirms that the proposed method is very accurate in estimating the simulated temporal variability.

Simulation 2: Spatial Registration. In the second simulation, we study the effectiveness of the spatial registration portion of the proposed method. Here, we generate two trajectories with small geometric variability in the form of a shifting peak on a circle for both inside and outside boundaries. But, to control the temporal variability we ensure that the average areas enclosed by the two boundaries along each trajectory are the same. Thus, only spatial registration is required in this case. The results of our alignment and comparison are presented in Figure 3. As expected, the proposed method does not perform any temporal alignment. The effects of the spatial alignment are clearly seen in panels (a) and (b). In (a), the linear interpolation between the two trajectories loses important features and re-

sults in distorted inside and outside shapes. In some cases, the shapes even contain two peaks, which is never present in the given data. This is not the case in panel (b) where the simulated peaks simply shift as one trajectory is deformed into another. This represents a more natural deformation. The distance between the original trajectories is 1.7177; it decreases to 0.8924 due to the spatial alignment using the proposed method. These improvements also manifest themselves in averaging of such trajectories.

Simulation 3: Spatio-temporal Registration. In this simulation, the two trajectories vary in both time and space. Again, the spatial variability comes from small geometric differences due to shifting peaks on circular inside and outside boundaries. The temporal variability is simulated by changing the circle radii in different manners across the two trajectories. In this example we are interested in the effectiveness of the proposed method to jointly register the temporal and spatial components of the two trajectories. The comparison is presented in Figure 4. First, we focus on the temporal alignment. Comparing panels (a) and (b), it can be clearly seen that there is temporal variability across the two red-blue trajectories. This is especially clear in the fourth row from the top. Panel (c) also clearly indicates a misalignment based on the average area functions. Prior to temporal alignment, the peaks for the two functions occur at approximately time $t = 0.5$ for trajectory 1 (blue) and $t = 0.85$ for trajectory 2 (red). The proposed method accounts for this by nonlinearly shifting the red function such that the peaks match, resulting in the green function. The temporal warping is given in (d). Next, we focus on the spatial variability. Again, without spatial alignment the linear interpolation between the two trajectories contains distorted features. After alignment, the deformations are more natural. In this example, the initial distance (without spatio-temporal alignment) was 2.0559. After alignment, the distance was 1.2169 (de-

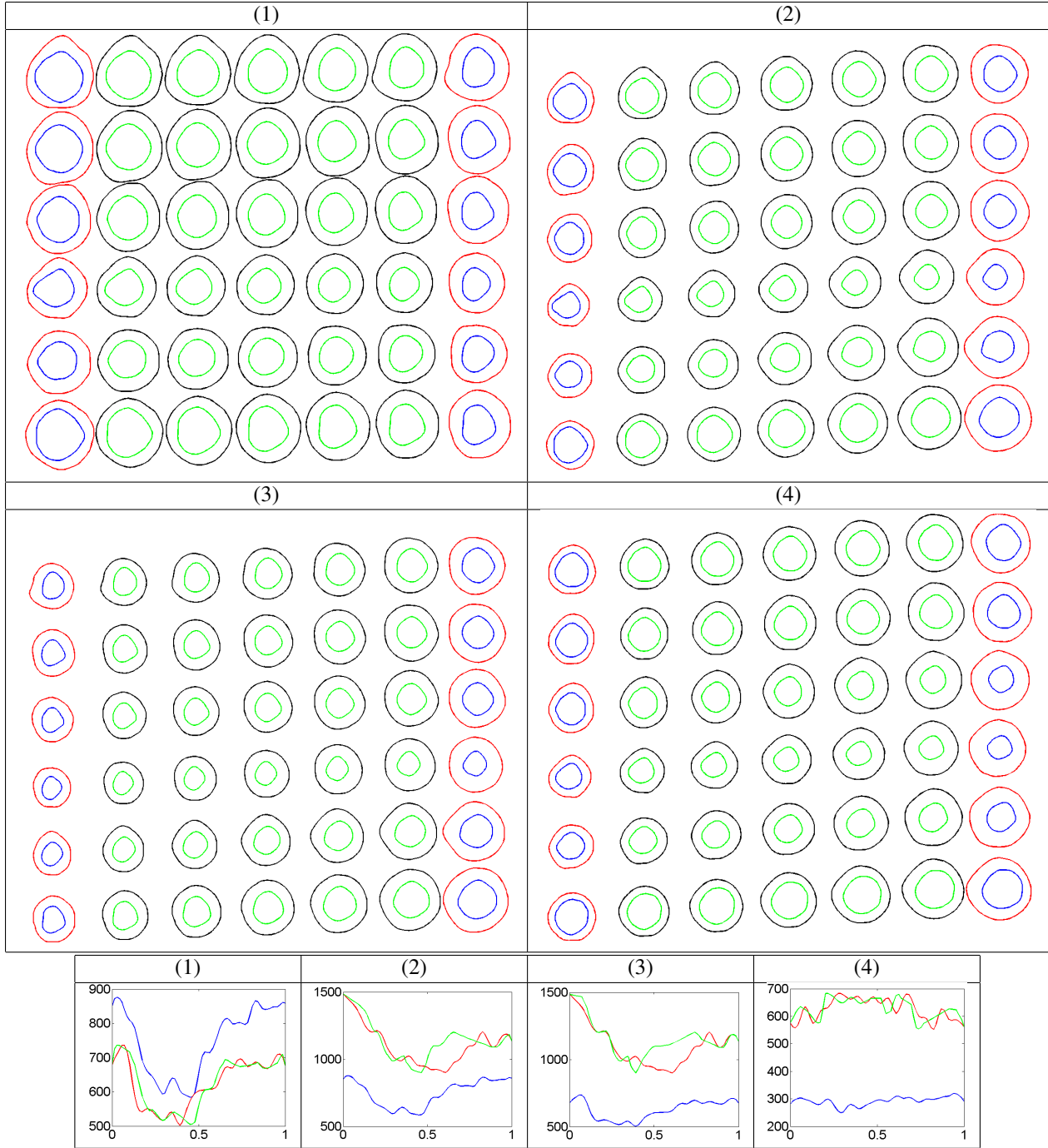


Figure 6. Top: Four comparisons ((1)-(4)) of myocardial trajectories using the proposed method. Each trajectory begins with $t = 0$ at the bottom of the plot and ends with $t = 1$ at the top of the plot with equal time sampling in-between. Bottom: Average area function for trajectory 1 (blue), trajectory 2 before alignment (red) and after alignment (green).

crease of over 40%).

Simulation 4: Trajectory Averaging. In the last simulation, we generate five different trajectories that vary temporally and spatially. We do not display these trajectories for brevity and note that they are of the same form as those in

Simulation 3. We compute an average trajectory using the proposed method and compare its spatio-temporal structure to a simple cross-sectional average without spatio-temporal registration. The results of this analysis are presented in Figure 5. From panels (c)-(e) it is evident that the pro-

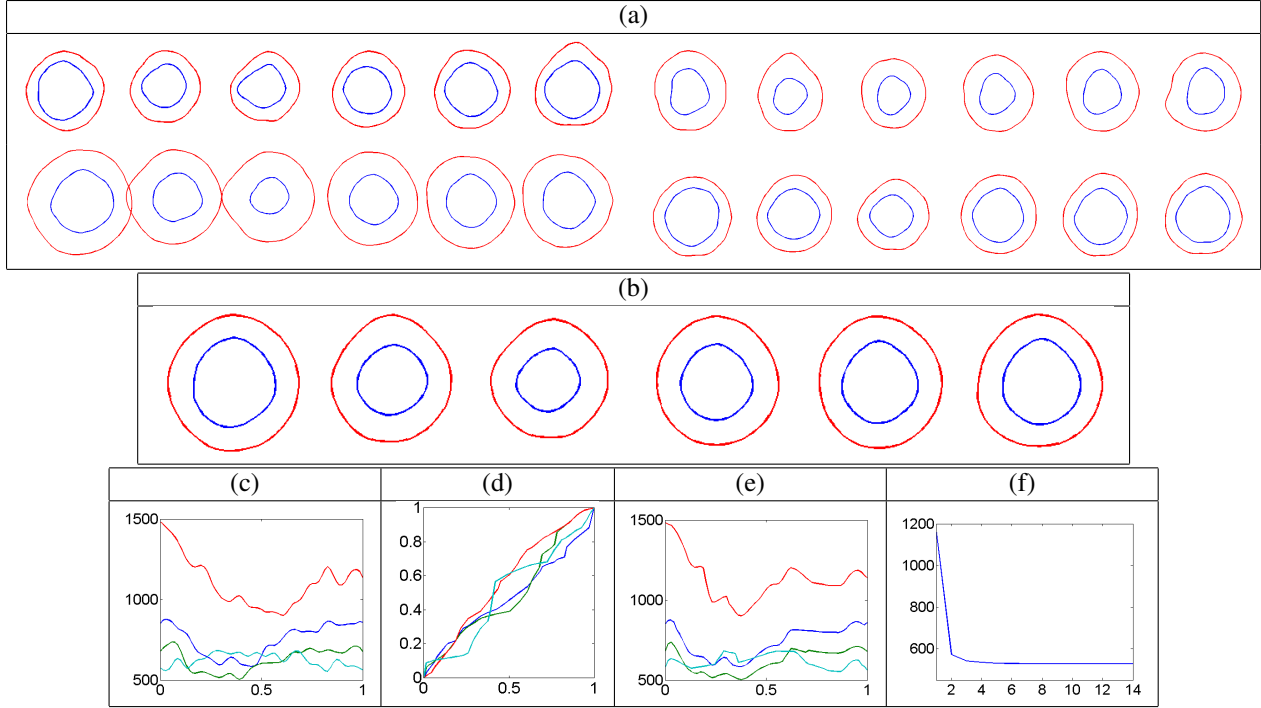


Figure 7. Averaging of myocardial trajectories. (a) Given sample. (b) Average computed using the proposed method. Each trajectory begins with $t = 0$ and ends with $t = 1$ (left to right). (c) Average area functions for the four trajectories prior to temporal alignment. (d) Temporal warping functions. (e) Average area functions after temporal alignment. (f) Evolution of the algorithm energy (variance).

posed method effectively accounts for the temporal variability based on the average area functions. The subsequent cross-sectional spatial averaging greatly improves the geometric structure of the inside and outside boundaries in the average trajectory. A naive average without spatio-temporal registration contains distorted features as displayed in panel (a). The average computed using the proposed method, shown in panel (b), contains sharp peaks and is a better representative of the original data. The decrease in the energy of the averaging algorithm as a function of the number of iterations is given in (f). The energy decrease is large due to the spatial registration performed by the proposed method.

4.2. Myocardial Trajectories from medical images

Here, we present four comparisons of myocardial trajectories extracted as endocardial and epicardial boundaries from cine MRI images during one cardiac cycle. In the bottom of Figure 6, we display the temporal registration results based on average area functions. It is noted that the alignment of peaks and valleys after temporal registration is significantly improved. The top portion of this figure displays the geodesic deformations between the spatio-temporally registered trajectories. It is more difficult to interpret these results in terms of the preservation of inside and outside boundary features along the deformation. Nonetheless, in each example, the distance decreases significantly due to

the additional spatio-temporal alignment of the trajectories: (1) 2.5243 to 2.2968, (2) 2.7234 to 2.5006, (3) 3.0279 to 2.8917, and (4) 3.9096 to 2.5702.

Finally, we present an example of averaging of four myocardial trajectories; the results are presented in Figure 7. The original sample is displayed in panel (a). Panel (b) shows the average myocardial trajectory computed using the proposed method. Panels (c)-(e) display the temporal registration results where a clear improvement in alignment of the average area functions is observed. Panel (f) shows the evolution of the average variance as a function of the number of iterations. As in the case of the simulated examples, we notice a significant decrease in the variance.

5. Summary and Future Work

We presented a new framework for spatio-temporal analysis of elastic shape trajectories based on the concepts of elastic functional data analysis and elastic shape analysis. The proposed method allows for joint registration, comparison and averaging of such trajectories. We evaluated our approach using simulated examples as well as real myocardial trajectories. In the future, we plan to focus on developing generative models for myocardial trajectories, which can be used for statistical simulation and tracking of the myocardium in cardiac pathologies.

References

- [1] A. Amini, Y. Chen, M. Elayyadi, and P. Radeva. Tag surface reconstruction and tracking of myocardial beads from spamm-mri with parametric b-spline surfaces. *IEEE Transactions on Medical Imaging*, 20(2):94–103, 2001.
- [2] A. Frangi, D. Rueckert, J. Schnabel, and W. Niessen. Automatic construction of multiple-object three-dimensional statistical shape models: Application to cardiac modeling. *IEEE Transactions on Medical Imaging*, 21(9):1151–66, 2002.
- [3] K. Hara and R. Chellappa. Generalized regression forests for continuous pose and direction estimation. In *European Conference on Computer Vision (ECCV)*, 2014.
- [4] G. A. Holzapfel and R. W. Ogden. Constitutive modelling of passive myocardium: a structurally based framework for material characterization. *Philosophical Transactions of the Royal Society of London A: Mathematical, Physical and Engineering Sciences*, 367(1902):3445–3475, 2009.
- [5] S. H. Joshi, E. Klassen, A. Srivastava, and I. H. Jermyn. A novel representation for Riemannian analysis of elastic curves in R^n . In *IEEE Conference on Computer Vision and Pattern Recognition (CVPR)*, pages 1–7, 2007.
- [6] S. Kurtek, A. Srivastava, and W. Wu. Signal estimation under random time-warpings and nonlinear signal alignment. In *Neural Information Processing Systems (NIPS)*, 2011.
- [7] C. Samir, S. Kurtek, A. Srivastava, and M. Canis. Elastic shape analysis of cylindrical surfaces for 3D/2D registration in endometrial tissue characterization. *IEEE Transactions on Medical Imaging*, 33(5):1035–1043, 2014.
- [8] A. Srivastava, E. Klassen, S. H. Joshi, and I. H. Jermyn. Shape analysis of elastic curves in Euclidean spaces. *IEEE Transactions on Pattern Analysis and Machine Intelligence*, 33:1415–1428, 2011.
- [9] A. Srivastava, W. Wu, S. Kurtek, E. Klassen, and J. S. Marron. Registration of functional data using Fisher-Rao metric. *arXiv: 1103.3817v2*, 2011.
- [10] J. Su, S. Kurtek, E. Klassen, and A. Srivastava. Statistical analysis of trajectories on Riemannian manifolds: Bird migration, hurricane tracking and video surveillance. *Annals of Applied Statistics*, 8(1):530–552, 2014.
- [11] A. Veeraraghavan, A. Srivastava, A. K. Roy-Chowdhury, and R. Chellappa. Rate-invariant recognition of humans and their activities. *IEEE Transactions on Image Processing*, 18(6):1326–1339, 2009.
- [12] H. Wu, P.-A. Heng, and T.-T. Wong. Cardiac motion recovery using an incompressible b-solid model. *Medical Engineering & Physics*, 35(7):958–68, 2013.
- [13] Y. Zhu, X. Papademetris, A. Sinusas, and J. Duncan. A coupled deformable model for tracking myocardial borders from real-time echocardiography using an incompressibility constraint. *Medical Image Analysis*, 14(3):429–48, 2010.